On the effect of a Gaussian firing rate function and propagation delays on the dynamics of a network of Wilson-Cowan populations
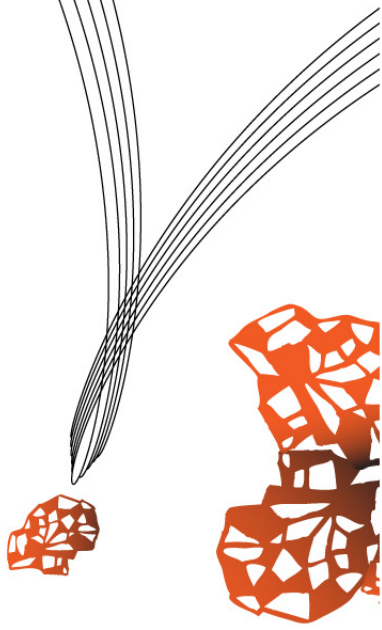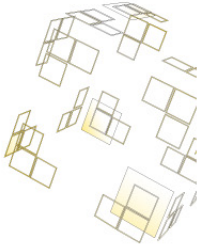
B. Kiewiet

Commitee:

Prof. Dr. S.A. van Gils
Dr. H.G.E. Meijer
Dr. J. le Feber

September 19, 2014

UNIVERSITEIT TWENTE.

Abstract

We study the effect of a Gaussian firing rate function on the dynamics of a neural network of coupled Wilson-Cowan equations. Bifurcation analysis shows that an extra stable high activity equilibrium exists in addition to the normal behavior. Two populations are coupled by their excitatory subpopulations and a bifurcation analysis shows periodic solutions, some of which are not found using the original equations. Simulations with a large network of coupled populations show activity spread from a stable high activity population which drives the network. Using a propagation delay between populations, we analyze the stability of the various periodic solutions. It is shown that the coupling strength and propagation delay have a large influence on the stability of these periodic solutions. We classify patterns and link their appearance with the coupling strength and time delay in a large network of populations.

CONTENTS

CHAPTER 1
INTRODUCTION

Worldwide almost 65 million people suffer from epilepsy, a neurological disease with characteristics that are currently difficult to understand. Epilepsy is a disorder characterized predominantly by recurrent and unpredictable interruptions of normal brain function called seizures, with a seizure a transient occurrence of signs and/or symptoms due to abnormal excessive or synchronous neuronal activity in the brain [1]. The disease can roughly be divided into two groups based on the type of seizures [2]: Generalized and focal epilepsy. Research into the disease is carried out either *in vitro* (human or animal tissue) or *in vivo* (animal or clinical studies). Computational models can be of additional help in understanding the disease.

A recent experiment that recorded local field potentials in the core of an epileptic focus using an array of micro-electrodes, showed a Gaussian relationship between the inverted low frequency component of the potentials (L-LFP) and a multi-unit firing rate metric (Figure 1.1).

Based on these experimental results we want to create a model that incorporates the Gaussian relationship and analyze the fundamental changes in the dynamics as a result of this different relationship.

The brain consists of a large number of widely connected neurons, with short- and long-range connections. Many models for individual neurons have existed for some time (e.g. [3; 4; 5; 6]) and have been analyzed extensively (e.g. [7; 8]). Since micro-electrodes measures the activity of thousands of neurons the details about individual neurons are omitted. Looking at a macroscopic level neurons form neuronal networks and epilepsy can be seen as the result of "odd" activity of an interconnected neural network [2]. Modeling this

Figure 1.1: Experimental recordings

experiment as a large number of neuron models is thus not required. Instead, Mean-field or neural mass models can be used to represent a large number of neurons. In this case results are more easily computed and interpreted than networks of a large number of single neuron models. With these type of models we look at the average behavior of populations of neurons. Many different neural mass models have been created (e.g. [9; 10; 11; 12; 13; 14]) and are most often described as nonlinear integral-differential equations. In this study we use the so called Wilson-Cowan equations as a basis to model our neural network.

Much mathematical analysis has been done on the equations since the model was first published in 1972 [15]. A bifurcation analysis shows the different types of behavior and bifurcations this simple model has [16]. The Gaussian relationship between the L-LFP and firing rate metric is modeled by switching the sigmoid for the Gaussian firing rate function in the equations. The firing rate function maps input current into a firing rate. Most neural mass models assume that single neurons begin firing, based on a mean threshold and some variance [17], and use a corresponding sigmoid or threshold firing rate function (e.g. [9; 12; 13]). Models for single neurons, however, show that with high input current, an individual neuron has a depolarization block at which the neuron stops firing [7; 18]. A Gaussian shaped firing function takes the block of neurons into account and maps high input current onto a low firing rate. The

effect of the shape of the firing rate function has been studied [19], but a Gaussian shaped function has not been used in this context.

Focal-onset start from a small region and spreads subsequently to other regions [1]. Additionally, recent micro-electrode array recordings showed that propagation of neural activity occurs at a spatial scale below the size of a conventional electroencephalogram (EEG) [20].This justifies the use of a spatially extended network of multiple Wilson-Cowan populations to model the seizure in addition to a temporal evolution. Networks of populations have been studied (e.g [21; 22; 23]) and showed spike-wave discharges and activity waves when networks were spatially coupled.

A modification of neural networks is the incorporation of delays [24; 25; 26]. The finite traveling speed of action potentials, transformations from electrical to bio-chemical signals and the spread of post-synaptic potentials in a neuron give reason to model spatially extended systems with time delays [27]. It has been shown that a delay can generate new dynamics not present without a delay. The micro-electrodes on the array are placed in a grid. We choose to incorporate a time delay in the model to represent the finite time an action potential needs to travel from one electrode on the grid to another.

In this study we look at a network of coupled Wilson-Cowan equations that uses a Gaussian firing rate function. The network has a propagation delay between populations and EEG output is modeled as the average current into three populations.

In chapter 2 we give the mathematical model. In chapter 3 we analyze the effect of using a Gaussian firing rate function in a network without propagation delays. The effect of incorporating a propagation delay between populations is studied in chapter 4. Finally, we discuss the results in chapter 5.

Research questions

In this study we try to answer the following questions:

- What is the effect of using a Gaussian firing rate function on the dynamics of the Wilson-Cowan model?

- What is the effect propagation delays between excitatory populations on the stability of periodic solutions in a network of Wilson-Cowan populations?

CHAPTER 2
MODEL DESCRIPTION

This study models a neuronal network as a set of coupled neural mass populations including spatial nearest neighbour interactions. Each local population is governed by the Wilson-Cowan equations, consisting of an excitatory and inhibitory subpopulation. The inhibitory subpopulation receives self-inhibition in addition to an excitatory current from the excitatory subpopulation. The excitatory subpopulation receives self-excitation, an excitatory current from its neighbors and an inhibitory current from the inhibitory subpopulation. Each current has a strength $w_{X \to Y}$ that translates activity into current. Propagation delays between the excitatory subpopulations is also incorporated. The Wilson-Cowan equations are given by:

$$\begin{cases} E_k' & = -E_k + (1 - E_k)F_E(J_{E_k}), \\ I_k' & = -I_k + (1 - I_k)F_I(J_{I_k}), \end{cases}$$

where $k = 1...N$ and the Gaussian firing rate functions (FRF) are given by:

$$\begin{cases} F_E(J_{E_k}) & = \exp\left(-\left(\frac{J_{E_k}-E_\theta}{E_{sd}}\right)^2\right) - \exp\left(-\left(\frac{0-E_\theta}{E_{sd}}\right)^2\right), \\ F_I(J_{I_k}) & = \exp\left(-\left(\frac{J_{I_k}-I_\theta}{I_{sd}}\right)^2\right) - \exp\left(-\left(\frac{0-I_\theta}{I_{sd}}\right)^2\right), \end{cases}$$

or in the sigmoid case:

$$\begin{cases} F_E(J_{E_k}) & = (1 + \exp\left(-Es_{Slope}\left(J_{E_k} - Es_\theta\right)\right))^{-1} - (1 + \exp\left(Es_{Slope}Es_\theta\right))^{-1}, \\ F_I(J_{I_k}) & = (1 + \exp\left(-Is_{Slope}\left(J_{I_k} - Is_\theta\right)\right))^{-1} - (1 + \exp\left(Is_{Slope}Is_\theta\right))^{-1}, \end{cases}$$

with input currents,

$$\begin{cases} J_{E_k} & = w_{EE}E_k(t) - w_{IE}I_k(t) + \alpha w_{EE}(E_{k-1}(t - \tau) + E_{k+1}(t - \tau)) + B, \\ J_{I_k} & = w_{EI}E_k(t) - w_{II}I_k(t), \end{cases}$$

where E_k and I_k are the activity of the kth excitatory and inhibitory subpopulations respectively. The functions $F_E(J_{E_k})$ and $F_I(J_{I_k})$ are the firing rate functions, which can be Gaussian shaped or sigmoid, with as argument J the input current for the specific subpopulation. The constants $w_{EE}, w_{EI}, w_{II}, w_{IE}$ weigh the activity from the different sources. All excitatory subpopulations receive the constant background current B. An additional coupling strength between excitatory subpopulations is given by α. The propagation delay τ between the excitatory subpopulations is the time that it takes for a signal to reach it neighbors. In the first part of this study this delay is zero. We model the EEG output as the average current. Figure 2.1 shows an schematic overview of the model and the values for the parameters are given in table 2.1.
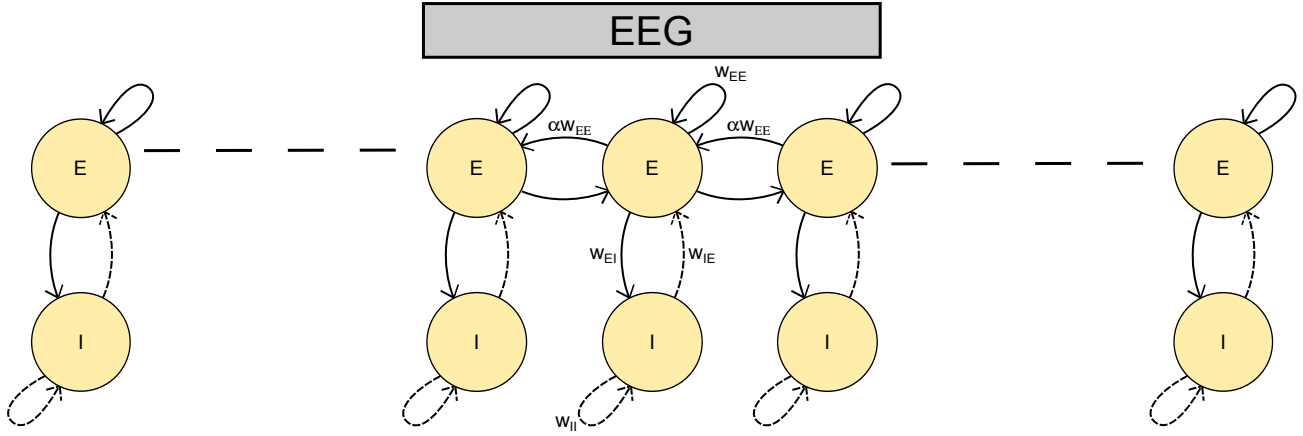
Figure 2.1: A schematic overview of the model. Each E-I pair is coupled, with or without propagation delay τ, to its neighbors through its excitatory subpopulation. We model EEG output as the average current over three populations. Solid: Excitatory connections; Dashed: Inhibitory connections.

Parameter	Description	Standard value	Varies
w_{EE}	Weight of current between excitatory populations	16	
w_{II}	Weight of feedback current of the inhibitory populations	3	
w_{IE}	Weight of current from inhibitory to excitatory populations	12	
w_{EI}	Weight of current from excitatory to inhibitory populations	18	x
E_θ	Mean of Gaussian FRF of excitatory populations	7	
I_θ	Mean of Gaussian FRF of inhibitory populations	5	
E_{SD}	Standard deviation of Gaussian FRF of excitatory populations	2.1	
I_{SD}	Standard deviation of Gaussian FRF of inhibitory populations	1.5	
Es_θ	Mean of sigmoid FRF of excitatory populations	5.2516	
Is_θ	Mean of sigmoid FRF of inhibitory populations	3.7512	
Es_{Slope}	Slope of sigmoid FRF of excitatory populations	1.5858	
Is_{Slope}	Slope of sigmoid FRF of inhibitory populations	2.2201	
B	Background current of excitatory populations	2.45 or 3	x
α	Connection strength between excitatory populations	0.1	x
τ	Propagation delay between excitatory populations	0	x

Table 2.1: The parameter values are based on earlier modeling studies [9; 10; 16; 21]. The values for the sigmoid FRF are chosen such that both FRFs have the same slope at half activitation.

CHAPTER 3
DYNAMICS WITH A GAUSSIAN FIRING RATE FUNCTION

In this chapter we discuss the effect of a Gaussian firing rate function (FRF) on the dynamics of the Wilson-Cowan (WC) populations. In the original WC equations it was assumed that each individual neuron had a threshold after which a neuron would respond to excitation and start firing. Integrating the firing rate of individual neurons over the relevant domain yields a sigmoid population FRF. If we incorporate the effect of an upper threshold for depolarization block the corresponding population FRF is Gaussian shaped. Here we assumed that after the upper threshold the individual neuron immediately stops firing. Figure 3.1 shows this result. Inhibitory cells are more easily activated than excitatory cells and thus the resulting firing rate functions are shifted to the left compared to the excitatory functions. The right figure shows the Gaussian and sigmoid functions used in our model. The parameters for the sigmoid are chosen such that the slope at the half activation point is identical to the Gaussian.

The WC equations are nonlinear and thus their dynamics can not be studied in the same way as with linear differential equations. In this report we use bifurcation theory to study the nonlinear Wilson-Cowan equations with a Gaussian FRF (WCG). Bifurcation theory in differential equations looks at the qualitative structure of the dynamics. By using bifurcation theory on dynamical systems we try to find the parameter values at which behavior changes qualitatively. For terminology and definitions of bifurcations we refer to [28]. A previous study computed a bifurcation diagram, using a sigmoid FRF, with the background current and the coupling from the excitatory to inhibitory population as free parameters. Using these two free parameters is adequate to describe the dynamics of a single $E - I$ pair. Indeed, with the background current as a free parameter we can directly influence the excitatory subpopulation, while with the excitatory to inhibitory coupling we can influence the inhibitory subpopulation, independently from the background input. In line with this study we make a bifurcation diagram, using the Matlab package Matcont [29], varying the same parameters and compare it to the bifurcation diagram with the fitted sigmoid curve. Phase plane portraits are made, using Pplane8 [30], for all regions with qualitative different behavior for the WCG equations. We use the bifurcation diagram and phase portraits to choose parameter values such that the effect of the Gaussian FRF is clear and oscillatory behavior is possible.

If two WCG populations are coupled, the interaction between them can generate new dynamics. The coupling strength between two WCG populations determines the amount of activity that is sent between the neighboring excitatory subpopulations. Bifurcation diagrams with the coupling strength as the active parameter are made for two cases with different background current. These diagrams will show the symmetry, stability and existence of equilibria and extrema of the periodic and quasi-periodic solutions. We study the effect of the Gaussian FRF on the dynamics of the coupled populations using time series and the bifurcation diagrams.

Based on the analysis done for a single and two coupled populations, parameters are selected and simulations are done for a large number of coupled WCG populations. In these simulations we will look at the existence of certain patterns and invariant sets in this larger network. For several simulations the average input current over 3 populations is plotted which models EEG output.
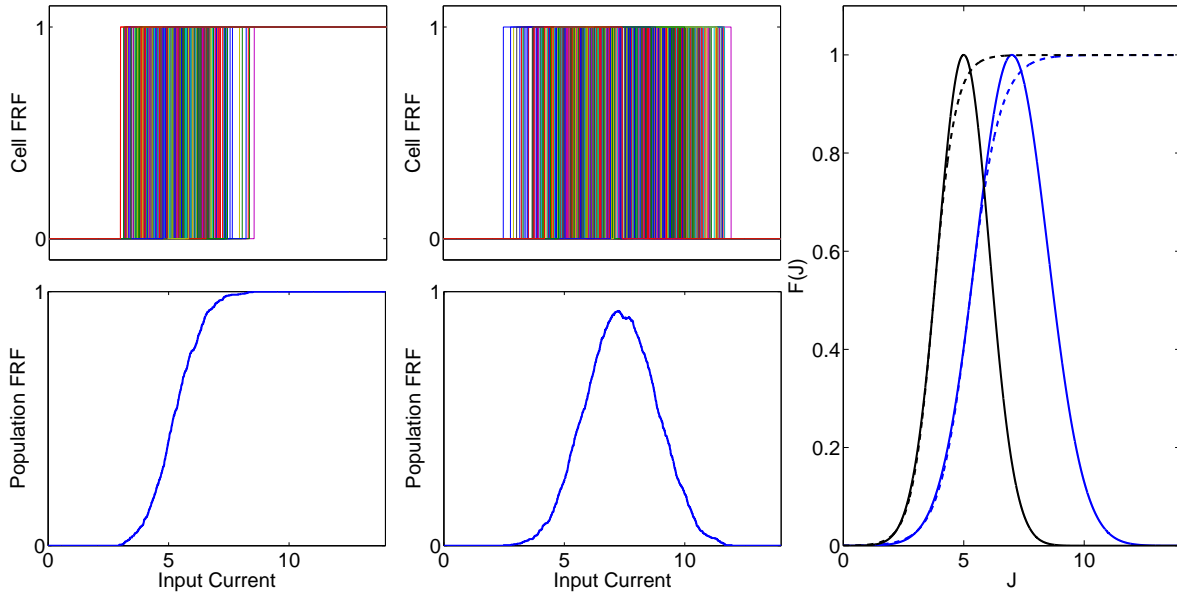
Figure 3.1: Left: Heterogeneity in firing onset for individual cells leads to a sigmoidal population FRF. Middle: Including the effect of heterogeneous thresholds for depolarization block leads to a population FRF with a maximum. Right: The FRFs used in this paper. Solid: Gaussian; Dashed: Sigmoid; Blue: Excitatory; Black: Inhibitory

3.1   A single E-I population

Here we look at a single E-I population. We first draw a comparison in the phase-planes of the WCG and the WC equations with the parameter values from table 2.1. Figure 3.2 shows the phase plane and their nullclines. The excitatory nullclines look similar in this region for the chosen parameter values except that for high values of E the nullcline turns more sharply. The inhibitory nullcline shows that with a Gaussian FRF the curve turns downward for high values of E. Due to this turn the inhibitory nullcline crosses the excitatory nullcline two more times compared to the sigmoid nullclines. The two resulting equilibria do not exist in the sigmoid case. Of the two extra equilibria one is a saddle and the other a stable node. The stable node has high excitatory and low inhibitory activity. The saddle has both high excitatory and high inhibitory activity.

The additional steady state is a robust feature coexisting with the normal dynamic repertoire of the WC model with a sigmoid FRF. Figure 3.3 shows for three different values of w_{EI} bifurcation diagrams for varying B with the excitatory activity on the vertical axis. The values of w_{EI} are chosen such that we cross several bifurcations in case B and C. In case A the dynamics are similar to the dynamics with a sigmoid FRF, because the high activity equilibrium does not exist for any value of B in addition to the normal dynamic repetoire.

Case A

For $B < 1.93$ the low activity equilibrium is the only equilibrium. At LP_1 two unstable equilibria appear via a fold bifurcation. At $SNIC$ another fold bifurcation removes the lower equilibria and all orbits converge to a stable limit cycle. At H we have a supercritical Hopf bifurcation and the limit cycle shrinks. At LP_3 and LP_2 we have two fold bifurcations and afterward only a
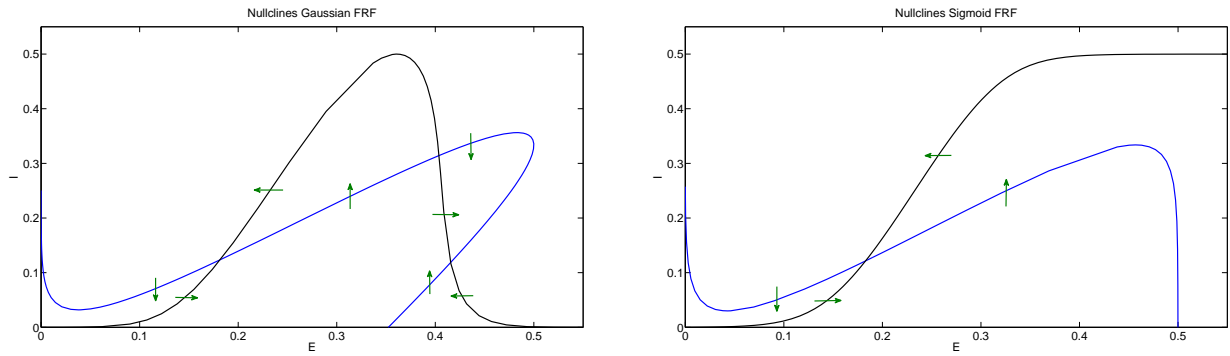
Figure 3.2: Nullclines and direction field for a Gaussian (left) and sigmoid (right) firing rate function. Parameters as in table 2.1 with $B = 3$ and $w_{EI} = 18$. Two additional high excitatory activity states exist in the Gaussian case

low activity equilibrium exists. Increasing B further the equilibrium converges to $(E, I) = (0, 0)$. The bifurcation diagram can be found in figure 3.3a.

Case B

For $B < -1.25$ the low activity equilibrium is the only equilibrium. At LP_1 we have a fold bifurcation and two high activity equilibria appear, of which the highest one is stable. Two unstable equilibria come into existence at LP_2 and at $SNIC$ the lower stable equilibrium disappears. All orbits then converge to a stable limit cycle or the high excitatory activity equilibrium. At $B = 4.693$ we cross a homoclinic bifurcation curve. An unstable limit cycle appears around the stable limit cycle and both limit cycles disappear when we cross a limit point of cycles curve (not indicated). At the fold bifurcation LP_4 two unstable equilibria disappear and all orbits converge to a high activity equilibrium. At LP_4 and LP_5 we have two more fold bifurcations that remove the high equilibrium and produce a low activity equilibrium respectively. If we increase B further the equilibrium converges to $(E, I) = (0, 0)$. The bifurcation diagram can be found in figure 3.3b.

Case C

For $B < -1.27$ the low activity equilibrium is the only equilibrium. At LP_1 we have a fold bifurcation and two high activity equilibria appear. At fold bifurcation LP_2 we have two new unstable equilibria of which one immediately has a supercritical Hopf bifurcation at H_1. At LP_3 two equilibria collide and disappear. Now all orbits converge either to the stable limit cycle or the high excitatory activity equilibrium. The limit cycle disappears at H_2 due to supercritical Hopf bifurcation. At $B = 5.197$ we cross a homoclinic bifurcation curve and an unstable limit cycle appears. At H_3 we have a subcritical Hopf bifurcation that removes the unstable limit cycle. The fold bifurcation LP_4 removes the unstable equilibria and all orbits converge to a high activity equilibrium. We have a new stable equilibrium at the fold bifurcation LP_5 and at the fold bifurcation LP_6 the high excitation equilibrium is removed. If we increase B further the equilibrium converges to $(E, I) = (0, 0)$. The bifurcation diagram can be found in figure 3.3c.
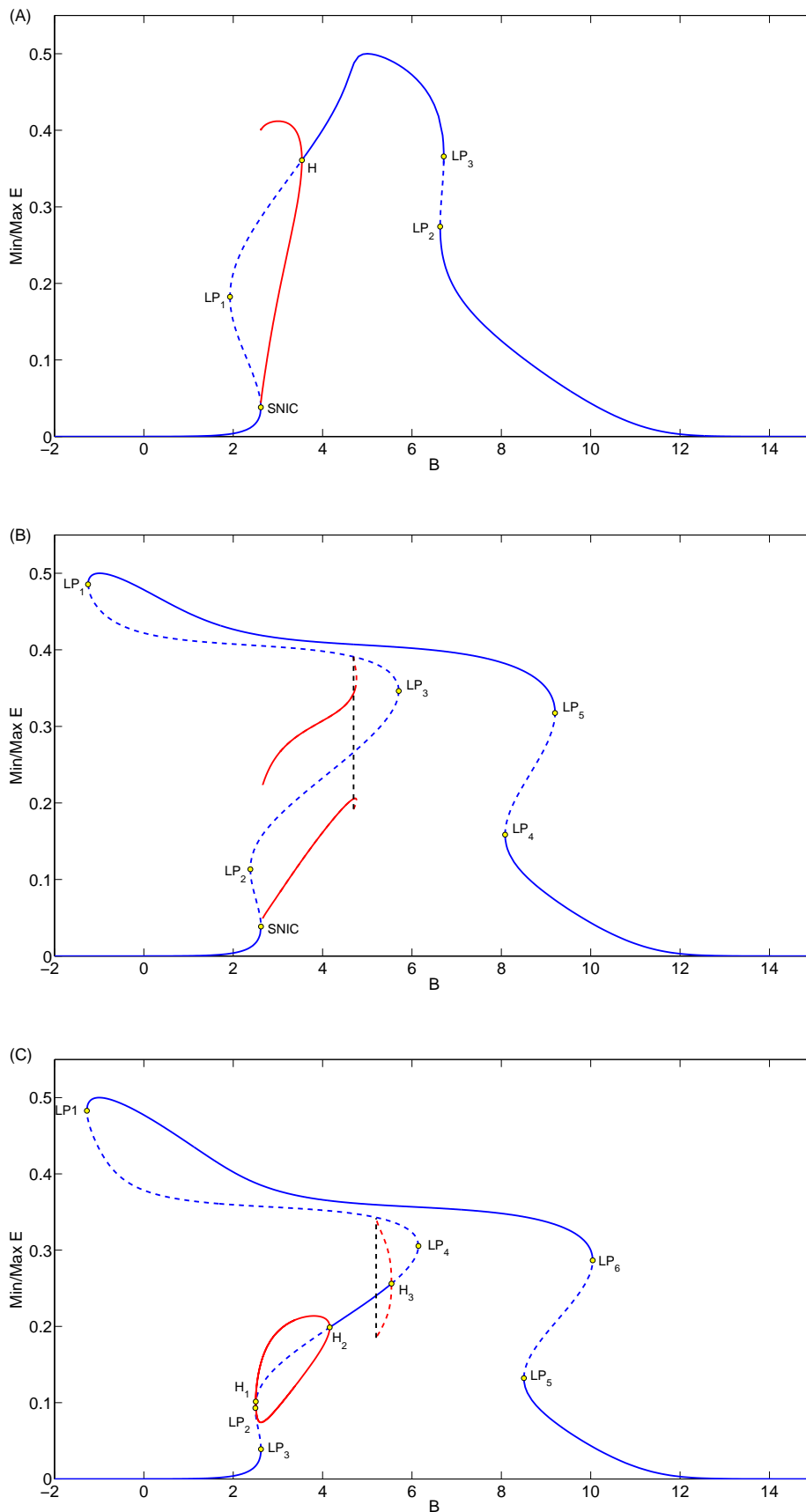
Figure 3.3: Bifurcation diagrams for $w_{EI} = 13$ (top), $w_{EI} = 18$ (middle) and $w_{EI} = 20.5$ (bottom) with a Gaussian FRF. Blue: Stable equilibrium; Red: Extrema of limit cycles; Solid: Stable; Dashed: Unstable. The dashed black line indicates a homoclinic bifurcation. By Increasing w_{EI} a fold bifurcation is crossed and two high activity equilibria appear. The dynamics if $w_{EI} = 13$ can also be found when a sigmoid FRF is used.

Full Bifurcation Diagrams

Figure 3.4 shows the bifurcation diagrams with background activity B and the coupling from the excitatory to inhibitory population w_{EI} as free parameters. With these free parameters we are able to show the main determinants of the dynamics, such as the existence of steady states and periodic oscillations.

For small values of w_{EI} the bifurcation diagrams of the WCG and WC equations look similar. For large values of w_{EI} we find in the Gaussian case an extra fold (saddle-node) curve that corresponds with the two extra high activity equilibria. At this fold curve we also find two Bogdanov-Takens points, which also exist in the sigmoid case but on a different fold curve corresponding to high values of B. From the Bogdanov-Takens (BT) point a Hopf curve emerges that ends at another BT point. On this Hopf curve there are degeneracies where the Hopf bifurcation changes from super- to subcritical. Here limit point of cycle bifurcation curves emerges that end in points where the saddle along a homoclinic curve is a neutral saddle (NH). The homoclinic curves emerging from a BT point either end in saddle-node homoclinics (SNIC) or connect to another BT-point.

For the Gaussian case a characteristic phase portrait is created for all 19 areas, see figure 3.5. Starting from area 1, we find a single stable low activity equilibrium. Crossing the fold bifurcation into areas 2 or 5 two equilibria appear. In area 2 they have high excitatory activity, while in area 5 the activity is low. Crossing another fold bifurcation into area 3 two equilibria collide and only a single stable equilibrium exists. In area 4 we have 3 equilibria with high excitatory and low inhibitory activity. In area 6 we find 5 equilibria of which 3 are stable. Going down into area 7 we cross a Hopf curve and a stable limit cycle appears with low activity. Into area 8 we go over a homoclinic curve and the limit cycle disappears. Down into area 9 we cross a fold curve and the two high excitatory activity equilibria collide and disappear. When we cross a homoclinic curve into area 10 a stable limit cycle appears. Crossing a homoclinic curve into area 11 gives rise to an unstable limit cycle around the stable limit cycle. Going from area 11 to 12 we cross a Hopf curve and the stable limit cycle disappears. In area 13 we find an unstable limit cycle and two high activity equilibria. Crossing the Hopf curve into area 14 a stable limit cycle appears inside the unstable cycle. Going into area 15 we cross a limit point of cycles curve and both limit cycles disappear. In area 16 we find a stable limit cycle and two high activity equilibria. Area 17 is equivalent to area 13 and crossing the homoclinic curve from area 17 into area 18 the unstable limit cycle disappears. In area 19 the only stable invariant set is the limit cycle. The areas in one of the sets $\{1,3\}, \{2,4,5,18\}, \{9,15\}, \{10,16\}, \{11,14\}$ and $\{12,13,17\}$ are all structurally equivalent. In total we have nine structurally different areas.

Effect of Gaussian FRF on a single population

The main effect of using a Gaussian FRF are the extra high activity equilibria in addition to the normal behavior we see in the original Wilson-Cowan equations. If the coupling strength between the excitatory and inhibitory subpopulations (w_{EI}) is large and the background input B not too big, then the current $J_I = w_{EI}E - w_{II}I$ is also large. The reverse is also true: If w_{EI} is small then the resulting current J_I is also small. Due to the symmetric shape of the Gaussian FRF and that w_{II} is relatively small, the resulting firing rate will be similar for the inhibitory subpopulation. This can be seen in the bifurcation diagram from the roughly similar shapes of the main curves and the large amount of structurally equivalent areas. Only areas 6,7 and 8 have low and high activity equilibria that coexist, because in those areas the main bifurcation curves overlap. The effect of the Gaussian FRF is most clear for $w_{EI} = 18$For this value we find from $B = 2$ to $B = 7$ several bifurcations as shown in figure 3.3b.
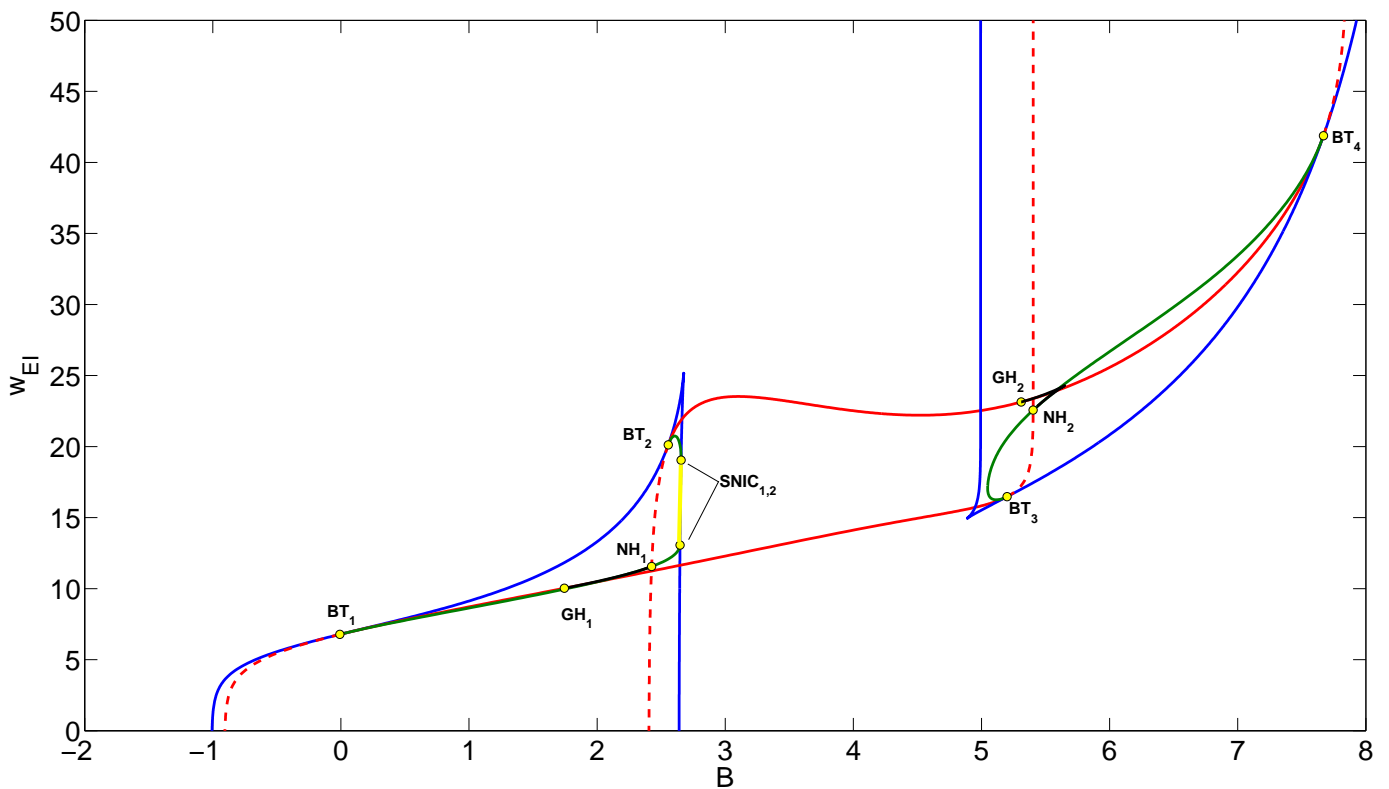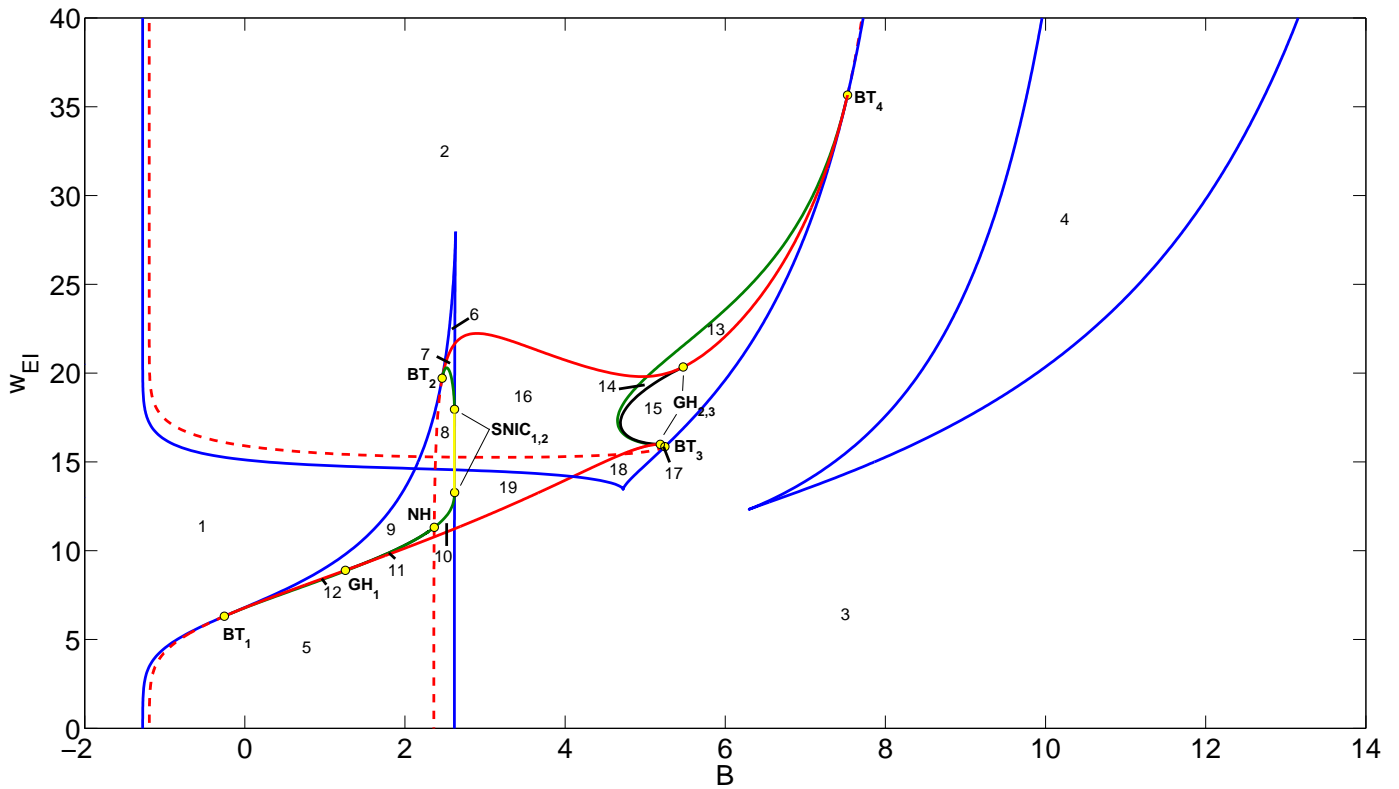
Figure 3.4: Bifurcation diagrams for Gaussian (top) and sigmoid (bottom) firing rate function, the active parameters are background input B and coupling parameter w_{EI}, other parameters as in table 2.1. Bifurcation curves are indicated with color: saddle-node (blue), Hopf (red), Limit point of cycles (black), Homoclinic to saddle (green), Saddle node on invariant curve (yellow). The red dashed line indicates a neutral saddle curve, which is not a bifurcation curve. Note the extra saddle-node curve for high values of w_{EI} and low values of B and the different horizontal scale.
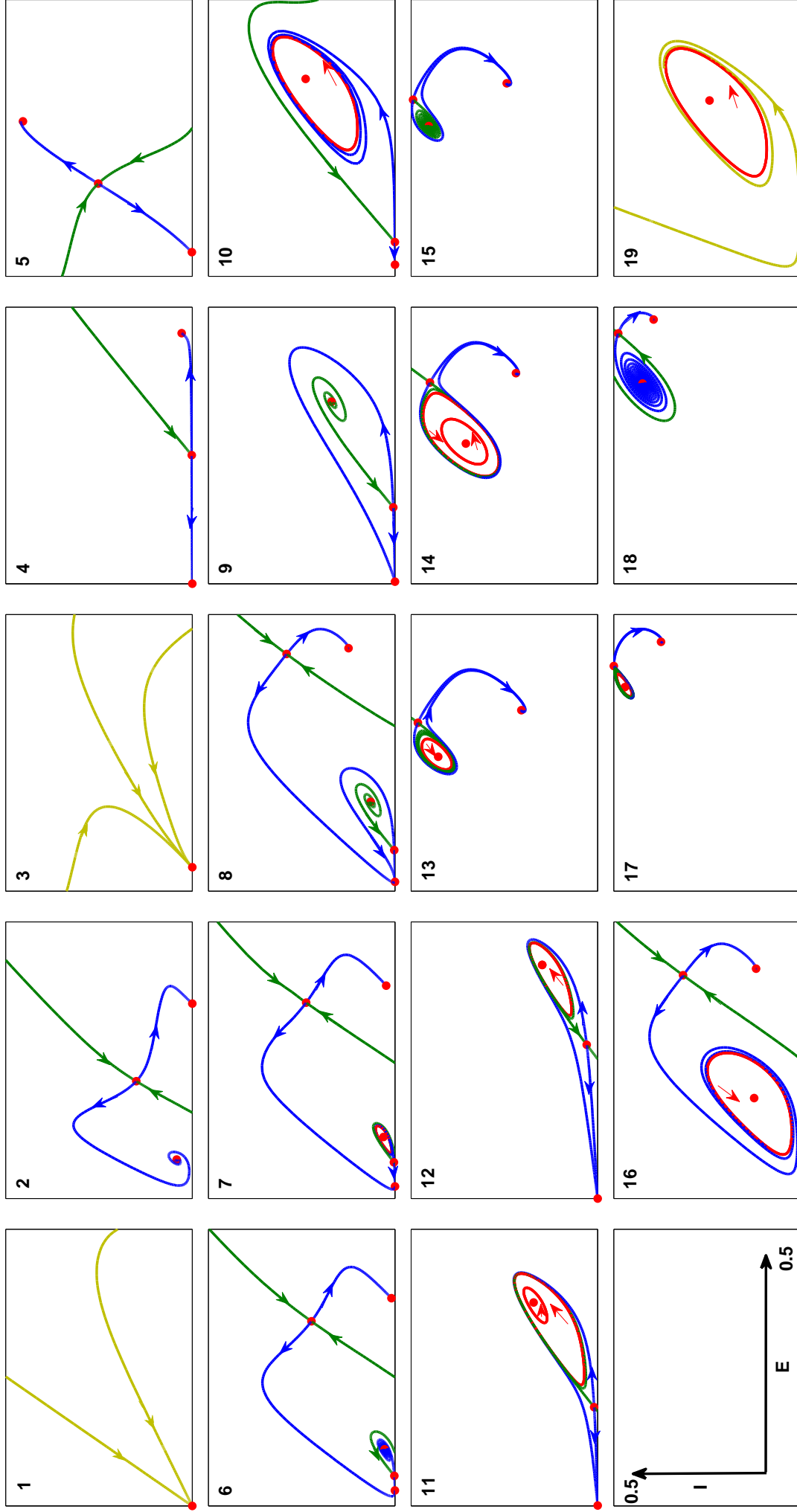
Figure 3.5: Phase portraits for all 19 regions. The numbers refer to the areas in figure 3.4. Red: Equilibrium or limit cycle; Green: Stable manifolds; Blue: Unstable manifolds; Yellow: Orbits. The areas in the sets {1, 3}, {2, 4, 5, 18}, {12, 13, 17}, {9, 15}, {10, 16} and {11, 14} are structurally equivalent.

3.2 Two coupled populations

Here we couple two populations by their excitatory subpopulations. We look at the impact of the coupling strength on the dynamics of the extended model. An extra parameter for the coupling strength, denoted by α, is introduced. The input current into an excitatory population then becomes: $J_{E_{ij}} = w_{EE}E_{ij} - w_{IE}I_{ij} + \alpha w_{EE}E_{ji} + B$ with $i, j \in \{1, 2\}, j \neq i$. Based on the analysis done for a single population we look at two cases: $B = 2.45$ and $B = 3$, with other parameter values as in table 2.1. Figure 3.6 shows bifurcation diagrams with the coupling strength α as the free parameter and the activity of an excitatory population on the vertical axis. Asymmetric branches forming from pitchfork bifurcations are linked, that is: If the upper branch corresponds to the population E_1, then the lower branch corresponds to the other population E_2 and vice versa.

We distinguish between symmetric and asymmetric invariant sets, anti-phase and in-phase periodic solutions and quasi-periodic oscillations.

Case A

Here we use $B = 2.45$. In this case the parameter set for both single populations corresponds to area 8 which has 5 equilibria of which two are stable. Activity from a neighboring population can push a population into area 2 or 16 depending on the value of α. Starting at the symmetric low activity equilibrium (black line) for $\alpha < 0$ we find at $\alpha = 0.332$ a fold bifurcation. Following the branch we find at $\alpha = 0.181$ a pitchfork bifurcation PF_1 which spawns two linked unstable asymmetric equilibria. Continuing the symmetric branch we find at $\alpha = -0.038$ a fold bifurcation. Shortly after we find PF_2 at $\alpha = -0.035$ which spawns another two linked unstable equilibria. At $\alpha = 0.115$ we find a Hopf bifurcation (not indicated) which creates an unstable symmetric limit cycle. We find at $\alpha = 0.607$ a fold bifurcation and PF_3 at $\alpha = 0.555$. The two new linked branches have a Hopf bifurcation and create an unstable limit cycle at $\alpha = 0.292$ before it disappears at $\alpha = 0.025$ due to a saddle-node homoclinic bifurcation. Continuing the black symmetric branch we have at $\alpha = -0.484$ a fold bifurcation and at PF_4 the symmetric equilibrium becomes stable again. Following the linked asymmetric equilibria we have LP_2 at $\alpha = 0.502$ where one equilibrium is stable. Around $\alpha = 0.2552$ the stable equilibrium undergoes a Hopf bifurcation H_2 and a stable limit cycle is created. The limit cycle disappears in a saddle-node homoclinic bifurcation at $\alpha = 0.025$. The unstable asymmetric curve has two fold bifurcations after it becomes stable again. The stable high activity symmetric equilibrium loses stability at PF_5. The linked asymmetric equilibria become stable at LP_3. The bifurcation diagram can be found in figure 3.6a.

Case B

Here we use $B = 3$. In this case the parameter set for both single populations corresponds to area 16. For $\alpha < 0$ we find two stable limit cycles, following the symmetric low activity equilibrium we find at pitchfork bifurcation PF_1 at $\alpha = -0.28$, which spawns two linked unstable asymmetric equilibria. At $\alpha = -0.115$ we have a Hopf bifurcation that spawns a limit cycle which becomes stable after the Neimark-Sacker bifurcation NS_1 at $\alpha = -0.04$ before losing stability again at $\alpha = 0$. At $\alpha = 0$ the two populations are decoupled and populations behave as individual populations in area 16. For $\alpha > 0$ an anti-phase periodic solution is stable until it loses stability at NS_2 with $\alpha = 0.044$. Here a quasi-periodic solution becomes an attractor. This attractor follows the curve of the unstable in-phase solution closely, but disappears slightly

earlier at $\alpha = 0.128$. This is because the attractor attains a higher maximum than the in-phase solution. At $\alpha = 0.1305$ the in-phase periodic solution disappears due to a homoclinic bifurcation. Continuing the symmetric branch we find at $\alpha = 0.5, -0.56$ fold bifurcations and at $\alpha = 0.465, -0.535, 1.047$ pitchfork bifurcations PF_2, PF_3 and PF_4. The corresponding linked asymmetric unstable branches are equivalent to those found at PF_3, PF_4 and PF_5 for $B = 2.45$ respectively. Between PF_3 and PF_4 the symmetric equilibrium is stable. The bifurcation diagram can be found in figure 3.6b.

Effect of the Gaussian FRF

For the linked asymmetric high-low activity stable limit cycle found for both $B = 2.45$ and $B = 3$ a time series is shown in figure 3.7. The figure also shows the input currents into the subpopulations and their dynamical range on the FRF. For the high activity population the excitatory and inhibitory subpopulation have high and low activity respectively, while for the low population both the excitatory and inhibitory subpopulations have both low activity. The excitatory subpopulations are in anti-phase while the inhibitory subpopulations are in-phase. This is due to the nature of the Gaussian function. If the inhibitory subpopulations receive enough activity to be on the right half of the Gaussian, then extra activity from the excitatory subpopulation is mapped onto a lower firing rate and thus less inhibitory activity. This also happens between the excitatory populations. If both subpopulations have a dynamic range on the left or right half on the Gaussian, they are in-phase or in anti-phase respectively.

This figure also shows why the high activity is stable. Suppose a population has high excitatory activity, then the inhibitory subpopulations receives a lot of input current since w_{EI} is large. This input current is mapped onto a small firing rate and thus the inhibitory activity is and stays small. The excitatory subpopulation then receives a small inhibition current and due to its self-excitation current stays at a high activity level. This high activity equilibrium is thus stable for a single population. Now suppose we receive an extra input current from a neighboring population while the population is in the high activity equilibrium. The current into the population is now larger and mapped onto a lower firing rate and thus the excitatory population becomes less active. This is counteracted by the self-excitation current. Lower activity means less self-excitation and thus the input current becomes smaller. This in turn is mapped on a larger firing rate and thus higher activity. The self-excitation and the neighboring current will balance themselves out and the population will settle on a slightly larger input current and corresponding lower activity. Indeed, figure 3.6b shows that the high excitatory activity of the unstable asymmetric equilibrium decreases if the coupling strength becomes larger.

A time series along with its projection on the (E_1, E_2) of the quasi-periodic solution from figure 3.6 is shown in figure 3.8. The time series suggest that the series first stays near the anti-phase solution, from which it escapes to the in-phase solution for a time and returns back to the anti-phase solution and so on. Increasing α, we find that the solution disappears via a global bifurcation and jumps to the high-low activity anti-phase solution.

(A)

B=3; w_EI=18

(B)
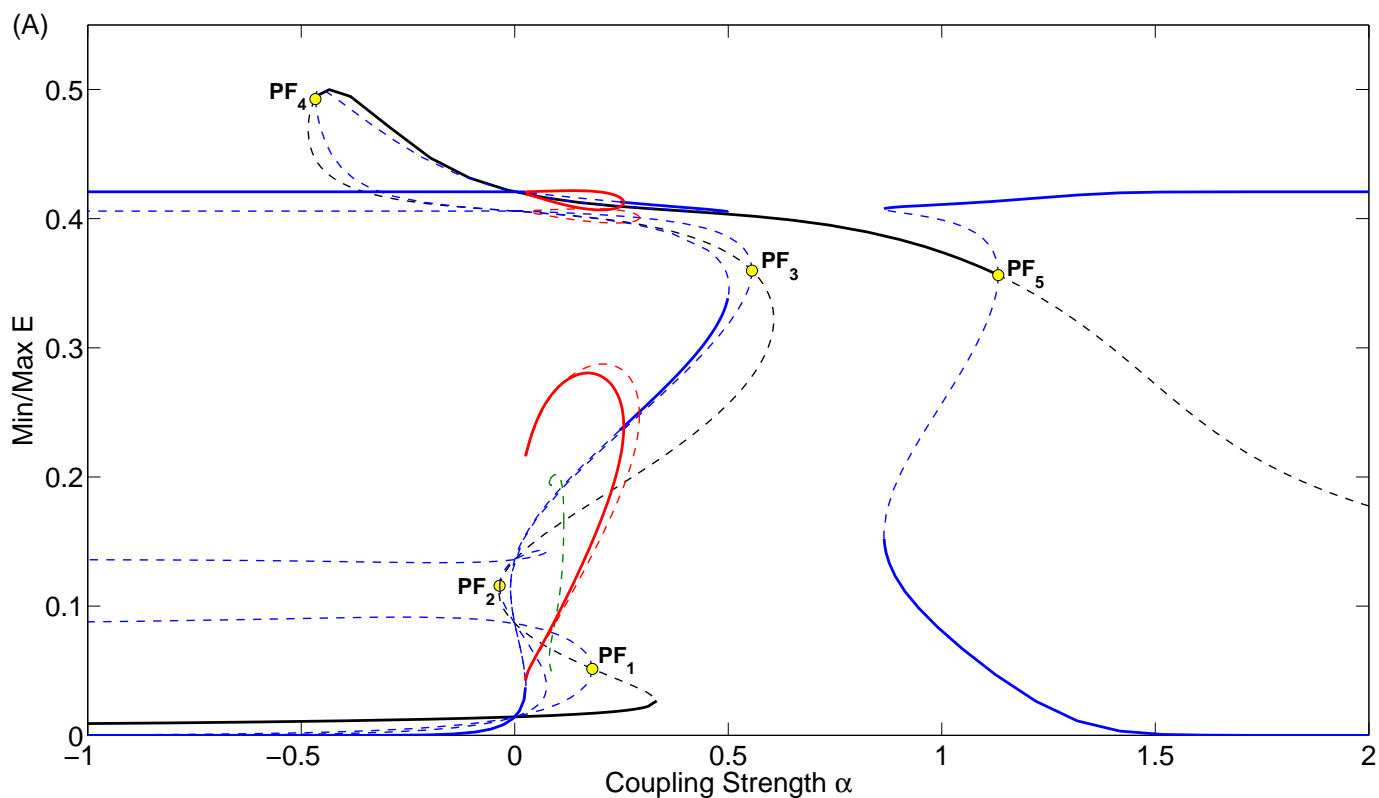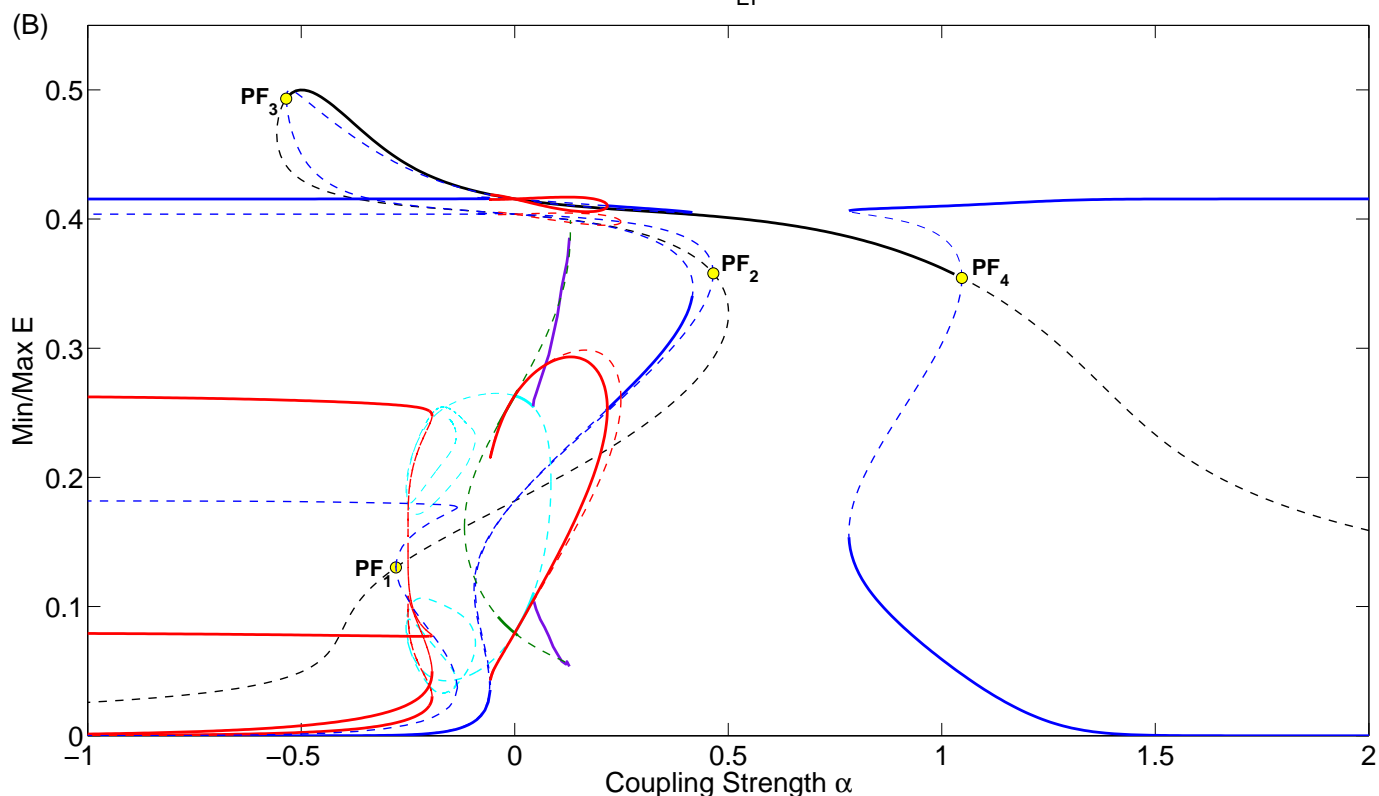
Figure 3.6: One parameter diagrams for $B = 2.45$ (top) and $B = 3$ (bottom). Black: Symmetric equilibria; Blue: Asymmetric equilibria; Green: Symmetric Oscillations; Red: Asymmetric Oscillations; Light blue: Antiphase Oscillations; Purple: Quasi-periodic oscillations. For the oscillations only the extrema are indicated. Thick solid and thin dashed lines indicate stable and unstable solutions respectively. At each pitchfork bifurcation (PF) two branches appear of which one corresponds to E_1 and the other to E_2 or vice versa.
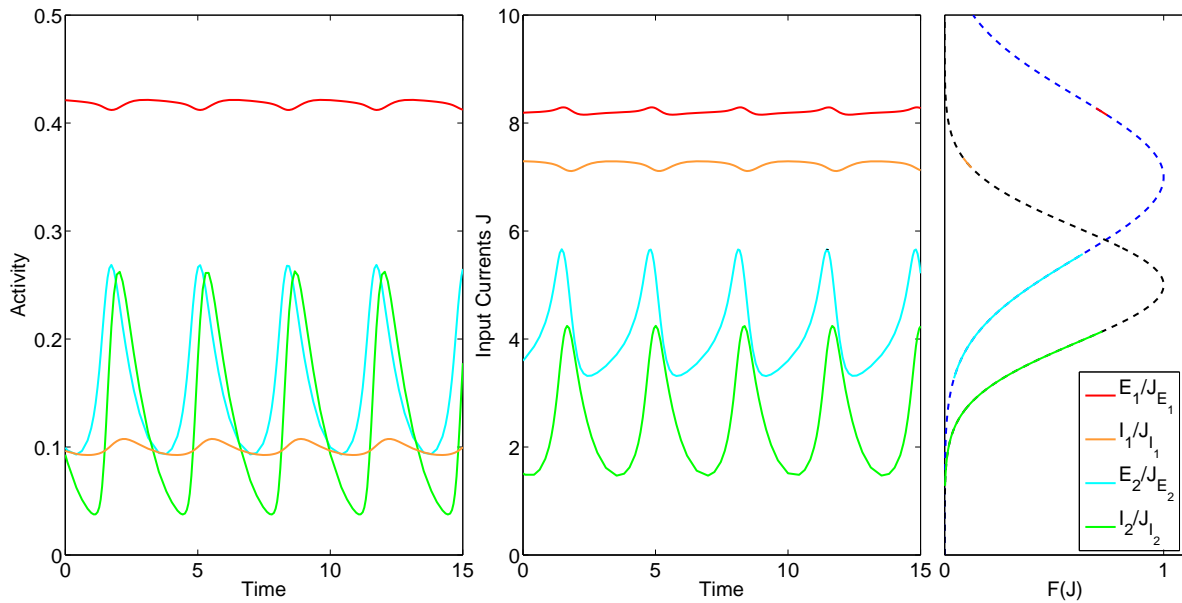
Figure 3.7: Left: Time series of the activity of the subpopulations for $B = 2.3$ and $\alpha = 0.1$; Middle: Input currents into each subpopulation; Right: The dynamical range of input currents J along the excitatory (blue) and inhibitory (black) FRF. Red: E_1; Orange: I_1; Light blue: E_2; Green: I_2. The high and low activity populations resides on the right and left halfs of the Gaussian FRF respectively.
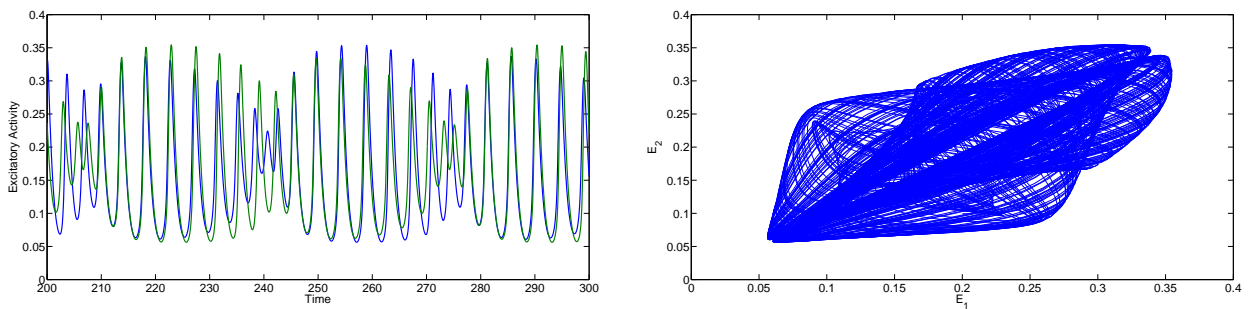
Figure 3.8: Left: Time series of the activity of excitatory populations of the quasi-periodic solution for $B = 3$ and $\alpha = 0.115$. Right: Projection to the (E_1, E_2) plane. When the torus is close to the symmetric oscillation, the projection is close to the diagonal $E_1 = E_2$.

3.3 Multiple populations

The previous sections showed that due to a Gaussian FRF a new high activity equilibrium exists. This equilibrium in turn forced its neighbor to oscillate as shown in the previous section. Here we use this high activity population as a driver to the whole neural network. All populations start in low activity and we stimulate one population enough to force it into the high excitatory activity stable equilibrium. The stimulated population is chosen such that it is next to the middle to avoid symmetry in the network. Figure 3.9 shows the spread of activity through the network.

For a background current $B = 2.3$ the populations are located in area 2 in figure 3.4 where the low and high activity equilibria are the only invariant sets. The high activity population provides sufficient input current to bring its neighboring populations into area 16, where only a stable limit cycle exists for low activity. These oscillations are not strong enough to force their neighbors into this area and thus the activity does not spread. If the background current $B = 2.45$ only a small additional current into a population is needed for it to start oscillating. Thus, oscillations start to ride on the background input. For large coupling strength α and large B, the network reaches a steady state in which the populations are active in an alternating pattern. This is a direct effect of the Gaussian FRF: Due to symmetry of the function high and low currents are mapped onto a similar firing rate. The high background current forces populations into the high activity stable equilibrium. The high coupling strength in turn forces the high activity populations into a depolarization block. These two mechanisms balance each other out and results in the alternating pattern. The right side of figure 3.9 shows the average of the input currents for the excitatory subpopulations over 3 neighbors. For $B = 2.45$ we see that every so many cycles three or more populations are activated and start oscillating. These waves end when they reach the boundary or when several populations are active simultaneously as occurs around $t = 152$ or $t = 183$. For the other two cases the output does not change spatially over time once stimulation is terminated.

The dynamics shown in 3.9 are a subset of all possible dynamics. Other dynamics such as the global low or global high activity equilibria correspond to the network being in a resting or highly active state respectively. Bumps in activity can also exist for several populations simultaneously. Each of these bumps drives the system and interactions between expanding activity generates new dynamics. The "random" activity pattern found in [22] also exist if a Gaussian FRF is used, because these dynamics coexist with the extra dynamics incorporated in the WCG network. The transient behavior and local extinction of activity in this pattern is related to the quasi-periodic solution seen in figure 3.8.
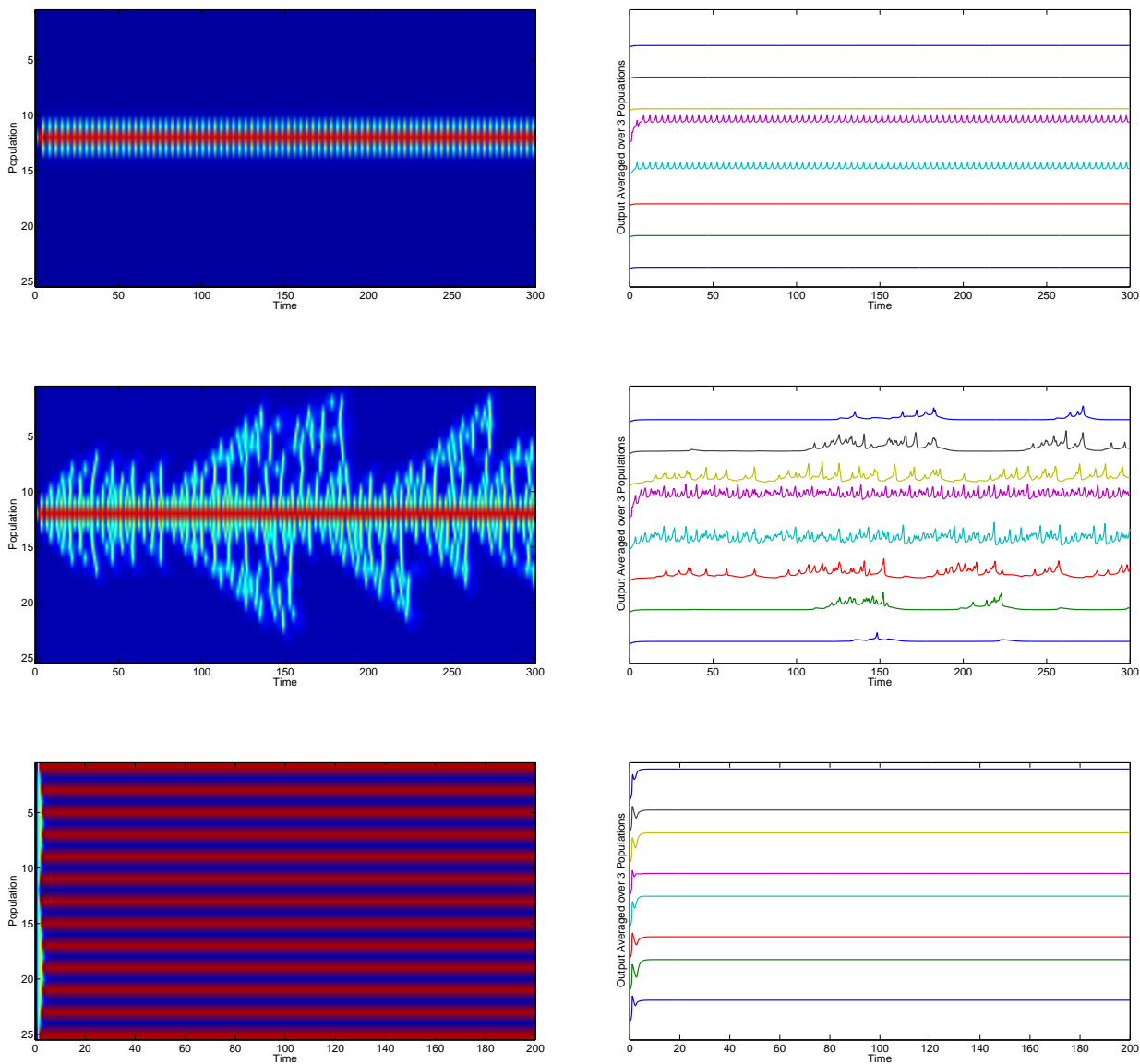
Figure 3.9: Left: Activity of excitatory populations after stimulation between $1 \le t \le 5$ with parameters $\{B = 2.3, \alpha = 0.1\}$ (top),$\{B = 2.45, \alpha = 0.1\}$ (middle) and $\{B = 3, \alpha = 0.6\}$ (bottom). Right: Input currents averaged over 3 populations. These simulations show new dynamics and invariant sets in the neural network made possible due to the Gaussian FRF.

CHAPTER 4
DYNAMICS WITH A PROPAGATION DELAY

In this chapter we study the effect of using a propagation delay for activity between populations on the dynamics of a network of Wilson-Cowan populations with a Gaussian firing rate function. The addition of a propagation delay turns the nonlinear WCG differential equations into delay differential equations. With a delay differential equation the derivative of a function depends on the state of the function some time ago, i.e. the history. In this model a fixed delay is used to transfer activity from one excitatory subpopulation to its neighbor(s). In the previous chapter we found different kinds of oscillations. Some of the oscillations only existed when a Gaussian firing rate function was used, such as the driving population and its oscillating neighbors. Other solutions also existed when a sigmoid firing rate function was used, such as the in-phase, anti-phase and quasi-periodic solutions. Depending on the background current and coupling strength between excitatory populations these solutions existed simultaneously with the high-low activity oscillations in the case of two coupled populations.

Here we will look at the existence and region of stability of the periodic solutions in a small network of two coupled populations with a propagation delay. We use the Matlab package DDE-BIFTOOL [31] to continue the periodic solutions in the time delay τ and coupling strength α and look at the stability. An analysis on the region of existence and stability is done and is compared to the system without a propagation delay.

Continuing the structure in the previous chapter we look at a large network of populations with a propagation delay. Simulations are made to link the results of the network of two coupled populations to this larger network. Different types of activity patterns are shown and classified. A classification diagram is made to show which dynamics are most prevalent for pairs of τ and α.

4.1 Two coupled populations

Here we look at two coupled populations with a propagation delay for transfering activity. Looking at the case without a propagation delay we find in-phase (IP), anti-phase (AP), a-periodic and high-low (HL) activity oscillations. Each of these oscillations exists in a certain parameter range of background current B and coupling strength α. In accordance to the structure of the previous chapter we determine the region of stability in two cases: $B = 2.45$ and $B = 3$. The region of stability is a subset of the region of existence. By simulating two populations, using $dde23$ in Matlab, we look for the periodic solutions for certain τ and α. In this study we chose to to scan the (τ, α)-space along 32 lines for $\tau = \frac{k}{4}$ with $k = 0...32$ and look at the stability of each computed point. Figure 4.1 shows the bounds in which the periodic solutions are stable for $B = 2.45$ and $B = 3$.

Case A

For $B = 2.45$ the HL solution is stable for all $\tau \in [0, 8]$. The upper bound for α changes with τ and the period is around 2. If α becomes too large the low activity population receives enough input current to jump to the high equilibrium and the periodic solution ceases to exist. The

upper bound for α in which the solution is stable is related to the period. The upperbound is at its maximum if the solution is in anti-phase a time length τ ago. Because the resolution of the grid is poor this is only roughly true for the peaks in the figure. The upper bound converges to $\alpha \approx 0.25$ if τ becomes large. The lower bound for $\alpha = 0.028$ comes from the homoclinic bifurcation and is also found in the case without a propagation delay. If the coupling strength is too small, the high activity population does not provide enough current for the low activity population to cross the bifurcation curve. The delay does not matter because the high activity equilibrium is stable without extra current from its neighbor. The AP solution is not stable for $\tau < 0.4$. For $\tau \in [0.4, 6.8]$ the lower and upper bounds of alpha show where the solution is stable. At $\alpha = 0.4$ and $\alpha = 6.8$ the periodic solution vanishes due to a homoclinic bifurcation. The IP solution does not exist for $B = 2.45$. The figure can be found in figure 4.1a.

Case B

For $B = 3$ the HL solution is stable. The existence does not depend on τ, but the stability boundary strongly on α. On the upper bound the period of the solution is around 2. The time delay between two peaks of the upper bound for alpha is approximately 1.5. The lower bound is smaller than zero and is not shown. The AP solution is stable for $\tau > 0$ depending on the value of α. The upper bound also slowly oscillates. At $\tau = 1$ the solution becomes stable for certain values of α. The region of stability for the IP solution looks similar to the region of the AP solution, but shifted to the right. A time delay of half a period corresponds to an input current of an anti-phase solution and explains their similarity . The lower bounds for the solutions are smaller than zero and not shown. Simulations, starting from random low activity history, show that the anti-phase and in-phase region of attractions change when the delay changes. Simulations for a certain parameter pair always go to either the anti-phase or the in-phase solution for low α. For intermediate α the quasi-periodic solution becomes dominant, while for large α the populations either go to the high-low periodic solution or the symmetric high activity equilibrium. The figure can be found in figure 4.1b.

Figure 4.2 shows the in-phase and anti-phase periodic solution. The activities are constant for the history $t \in [-\tau, 0]$ and are chosen randomly with $E_k, I_k \in [0, 0.25]; k = 1, 2$. The time series converges to the in-phase or anti-phase solutions. For these parameter values the region of attraction of the anti-phase solution is much larger. This is one of the few regions in which solutions for both the anti-phase as in-phase solutions could be found.
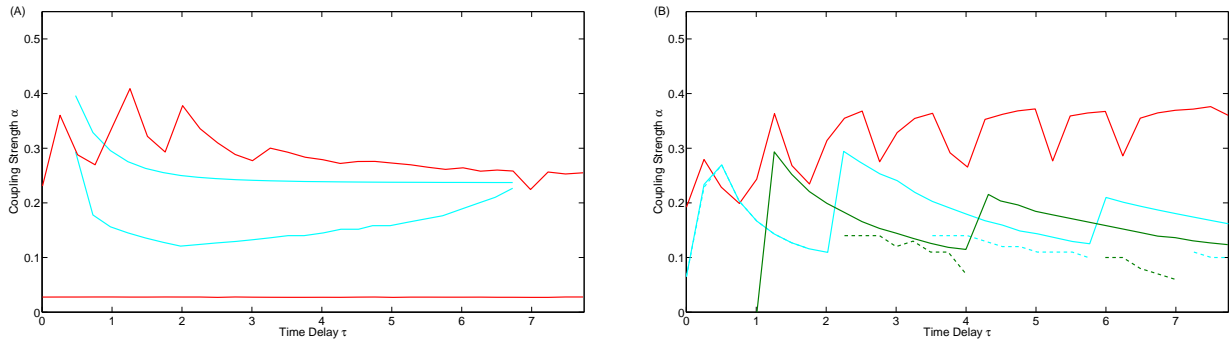
Figure 4.1: The lines indicate the upper and lower bounds in between which the periodic solutions are stable with $B = 2.45$ (left) and $B = 3$ (right). Stability was calculated at $\tau = 0.25k$ with $k = 0...32$ and lines were drawn between the points. The dashed lines in the right figure are the upper bound in which simulations showed in-phase or anti-phase solutions. If $B = 3$ the lower bounds are smaller than zero and not shown. Note that the solid and dashed lines only overlap for $\tau < 2$. Red: High-low activity; Green: In-phase low activity; Light blue: Anti-phase low activity.
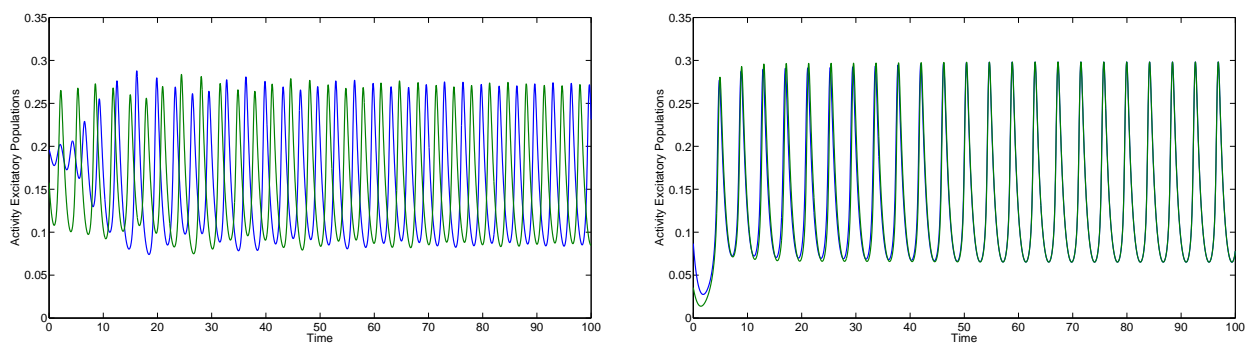
Figure 4.2: Time series for the anti-phase (left) and in-phase (right) solutions for $\alpha = 0.05, \tau = 4$ starting from random low activity history.
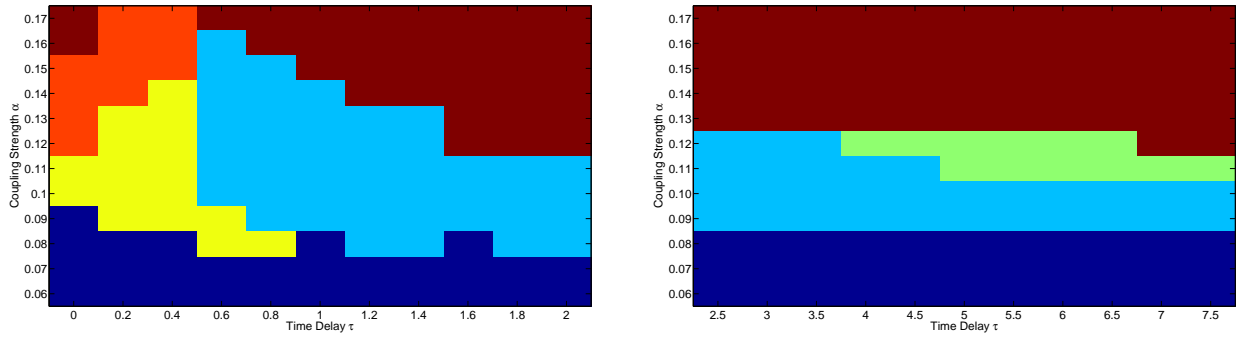
Figure 4.3: Classification of patterns after starting from random low activity history for various τ and α. Left: Small time delay; Right: Large delay. The figure on the left shows that quasi-periodic and bump activity disappears for a medium delay. The right figure shows that the in-phase solution becomes stable for a large delay. Dark blue: Low stable equilibrium; Yellow: Quasi-periodic; Light blue: Anti-phase; Green: In-phase; Red: Local bump in activity; Dark Red: High activity for all populations.

4.2 Multiple populations

The regions of stability found in the two populations do not directly transfer over to a network with multiple (> 2) populations, since in a larger network a population receives input current from two neighboring populations. An analytic approach to analyzing this network is outside the scope of this study, due to the computational requirements needed for all the computations. Instead we classify patterns and record their appearance for a range of values of α and τ.

We simulate 25 connected populations with the boundary populations connected to each other, thus the network forms a circle. Each population starts with random low activity history ($E_k(t), I_k(t) \in [0, 0.25]$ for $t \in [-\tau, 0]$ with $k = 1...25$). For each $\{\tau, \alpha\}$ pair 4 simulations are made and each pair is classified according to the most prevalent dynamics. For the classification we looked at the state the network was in for $t \in [100, 200]$. In the case that certain activity patterns coexist more simulations were done to determine a dominant pattern. Nonetheless this classification method only gives a qualitative estimate for certain patterns to appear.

In figure 4.3 we show the classification for each $\{\tau, \alpha\}$ pair. We distinguish between the patterns found in figure 4.4 in addition to the global low and high activity equilibria. For a small time delay $\tau < 0.6$ we see that the quasi-periodic and activity bump pattern are prevalent for low and high α respectively. Around $\tau = 0.6$ we see that the anti-phase pattern becomes dominant for medium α. If we increase τ further we see that the global high activity equilibrium becomes more dominant for a larger range α at the expense of the anti-phase pattern. The classification does not change much until we reach $\tau = 4$ where the in-phase solution becomes common in the simulations for a small range of α.

Figure 4.4 shows the patterns the can appear for various τ and α in addition to the global low and high activity equilibria. Figure 4.4a shows local bumps in activity. These bumps are stable and drive the system and can be linked to the HL periodic solution in the two population case. Figures 4.4b and 4.4c show the anti-phase and in-phase pattern. Their period increases with the time delay. The more chaotic pattern in the figure 4.4d could come from the quasi-periodic solution found in the analysis of two population without delay. We see that if populations synchronize locally activity extinguishes. Examples of this synchronization can be

25

found at $t = 60, 160$. The quasi-periodic solution from Figure 3.8 for two populations showed that the populations approach the in-phase before returning to the anti-phase solution. This could explain the synchronization in the larger network. If populations synchronize they reach their minimum in oscillations at the same time and do not receive enough input currents from its neighbors to keep oscillating.
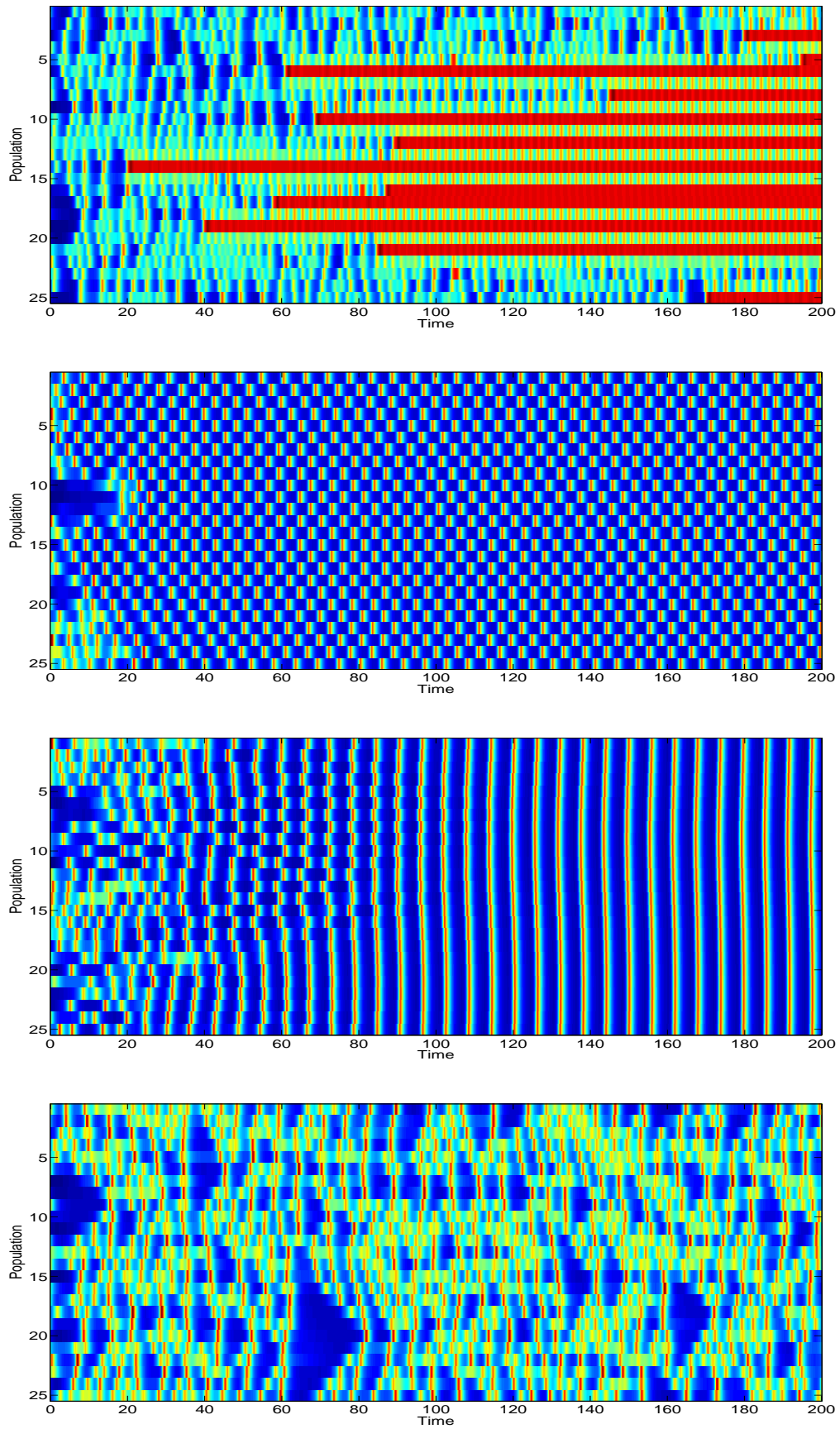
Figure 4.4: Different patterns in a neural network for (a) $\{\alpha = 0.15, \tau = 0.2\}$, (b) $\{\alpha = 0.12, \tau = 2\}$, (c) $\{\alpha = 0.12, \tau = 5\}$ and (d) $\{\alpha = 0.12, \tau = 0.2\}$

CHAPTER 5
DISCUSSION

In this study we have investigated the dynamics of a neural network governed by the Wilson-Cowan equations. In particular, we have chosen a Gaussian firing rate function, rather than the default sigmoid. Also, a propagation delay between the excitatory subpopulations was added. Some of the attractors we found using bifurcation analysis have been found in earlier studies for the case with zero propagation delay. When a Gaussian shaped firing function is used, an additional high activity is shown to exist. With multiple coupled populations this high activity population provided enough drive for surrounding populations to start oscillating. For certain parameter ranges one driving population could spread activity throughout the whole network.

The Gaussian firing rate function was motivated by observations of ictal activity using a Utah array. An experimental firing rate function could be determined using the low-frequency component of the local field potential to represent synaptic input, and the high-frequency component as spike output. For some cases this showed a nonmonotone relationship suggesting the choice for the Gaussian function. The experimental curve with low-frequency local field potential (L-LFP) plotted versus the high frequency components as a firing rate index suggests that beyond the maximum a plateau is reached, not unlike a depolarization block. For simplicity we have modeled the firing rate function as a Gaussian such that it returns to zero for high input current. With a certain set of parameter values, chosen such that the influence of the Gaussian FRF became most clear, an additional equilibrium with high excitatory and low inhibitory activity was found. This equilibrium coexists with the usual dynamics found in the sigmoid case. In this high activity equilibrium the inhibitory population receives enough input current and the inhibitory firing rate is low due to the shape of the FRF. This inhibitory firing rate is low enough for the excitatory population to receive low inhibition and thus remain highly active. This behavior of the inhibitory subpopulation could be seen as a depolarization block on a neural mass level. Due to the Gaussian shape the activity and input current vary much. Oscillating high activity populations receive an large input current with low amplitude, while its oscillating neighbors receive a relatively small input current with large amplitude.

The dynamic range of the excitatory firing rate function was just after the peak in the Gaussian, not unlike the experimental curve. The nullclines of a single E-I pair show that the Gaussian shape of the inhibitory subpopulation is more important than the shape of the excitatory subpopulation. A sigmoid firing function for the excitatory population would probably suffice to create similar dynamics, since the shape of the nullcline is not qualitatively different from the Gaussian one in the used domain.

The bifurcation analysis for two coupled local populations without propagation delay showed multiple stable attractors. In-phase, anti-phase and quasi-periodic periodic solutions have been found around a low steady state, their existence depending on the coupling strength α. These periodic solutions also exist in the sigmoid case. Another asymmetric stable equilibrium in which one population has high activity and the other low activity exist for high and low coupling strength. If an intermediate coupling strength is used the lower population starts to oscillate which forces the high activity to oscillate as well. The high and low activity oscillations have a small and large amplitude respectively. This stable equilibrium and periodic solution does not exist when a sigmoid function is used. In a larger network of coupled populations this equilibrium or periodic solution can act as a driving force to nearby populations.

We explored with a propagation delay between the excitatory the subpopulations region of stability for periodic solutions. The in-phase low activity solution became stable if a large propagation delay was added for small background currents. The stability region of the linked high and low activity oscillations resonated with the period of the oscillations. The existence of these oscillations depend only the coupling strength and not on the delay. The stability of each periodic solution is computed on a low resolution grid and thus results are not exact. Also no differentiation has been made between the different kind of bifurcations these periodic solutions have. Simulations showed that the region of attraction of the in-phase and anti-phase changed with the delay. The quasi-periodic attractor has a large region of attraction for parameter ranges in which both the in-phase as anti-phase solutions are stable.

For larger networks with propagation delay, a link was created between the time delay, coupling strength and the different kinds of stable patterns. With a small delay the quasi-periodic and local bumps in activity are the dominant patterns. For intermediate coupling strength and intermediate or high propagation delay the low activity anti-phase solution is the most dominant. Although the in-phase solution is stable, the anti-phase solution has a larger region of attraction for all but a few parameter ranges. Considering this, the effect of a propagation delay is important for the region of attractions in neural networks. The quasi- periodic solution for intermediate coupling strength exists in both the sigmoid as in the Gaussian case. The nature of this solution could explain the "random" times local extinction of activity occurs, since the solution skirts close to the in-phase solution, in which case the activity dies out locally if the background input is small. A further study of the nature of this solution could be done.

Epilepsy is characterized by transitions between normal and ictal activity. Although for certain parameter ranges our model produces transient activity, as with the quasi-periodic solutions, in general the model does not provide internal means to switch between those states. The different patterns found in the larger network are very stable and transitions between them are rare. Global parameter transitions however, could force a switch between different states. Influential parameters are the background current B, local connectivity w_{EI} and coupling strength α. Local or global stimulation patterns, adaptation and synaptic plasticity between subpopulations or populations could force transitions between states through new dynamics.

The actual micro-electrode array used in the experiments uses a 2D grid with electrodes. In our model however, we use a 1D grid. A study using the sigmoid firing rate function showed some possible dynamics of the network [22]. Here an external oscillation introduced to the center population formed waves of activity. With a Gaussian function a driving population instead could produce waves of activity throughout the system.

REFERENCES

[1] R. S. Fisher, W. Van Emde Boas, W. Blume, C. Elger, P. Genton, P. Lee, and J. Engel Jr., "Epileptic seizures and epilepsy: Definitions proposed by the international league against epilepsy (ilae) and the international bureau for epilepsy (ibe)," *Epilepsia*, vol. 46, no. 4, pp. 470–472, 2005.

[2] F. H. L. Da Silva, J. A. Gorter, and W. J. Wadman, *Epilepsy as a dynamic disease of neuronal networks*, vol. 107 of *Handbook of Clinical Neurology*. 2012.

[3] R. FitzHugh, "Impulses and physiological states in theoretical models of nerve membrane," *Biophysical Journal*, vol. 1, no. 6, pp. 445 – 466, 1961.

[4] N. Fourcaud-Trocmé, D. Hansel, C. Van Vreeswijk, and N. Brunel, "How spike generation mechanisms determine the neuronal response to fluctuating inputs," *The Journal of neuroscience*, vol. 23, no. 37, pp. 11628–11640, 2003.

[5] A. L. Hodgkin and A. F. Huxley, "A quantitative description of membrane current and its application to conduction and excitation in nerve.," *The Journal of physiology*, vol. 117, no. 4, pp. 500–544, 1952.

[6] N. F. Rulkov, "Modeling of spiking-bursting neural behavior using two-dimensional map," *Phys. Rev. E*, vol. 65, p. 041922, Apr 2002.

[7] E. M. Izhikevich, *Dynamical systems in neuroscience*. MIT press, 2007.

[8] J. Rinzel, "Discussion: Electrical excitability of cells, theory and experiment: Review of the hodgkin-huxley foundation and an update," *Bulletin of Mathematical Biology*, vol. 52, no. 1, pp. 5–23, 1990.

[9] H. R. Wilson and J. D. Cowan, "Excitatory and inhibitory interactions in localized populations of model neurons," *Biophysical journal*, vol. 12, no. 1, pp. 1–24, 1972.

[10] H. R. Wilson and J. D. Cowan, "A mathematical theory of the functional dynamics of cortical and thalamic nervous tissue," *Kybernetik*, vol. 13, no. 2, pp. 55–80, 1973.

[11] F. H. Lopes da Silva, A. Hoeks, H. Smits, and L. H. Zetterberg, "Model of brain rhythmic activity. the alpha rhythm of the thalamus," *Kybernetik*, vol. 15, no. 1, pp. 27–37, 1974.

[12] B. H. Jansen, G. Zouridakis, and M. E. Brandt, "A neurophysiologically-based mathematical model of flash visual evoked potentials," *Biological cybernetics*, vol. 68, no. 3, pp. 275–283, 1993.

[13] F. Wendling, F. Bartolomei, J. J. Bellanger, and P. Chauvel, "Epileptic fast activity can be explained by a model of impaired gabaergic dendritic inhibition," *European Journal of Neuroscience*, vol. 15, no. 9, pp. 1499–1508, 2002.

[14] S.-I. Amari, "Homogeneous nets of neuron-like elements," *Biological Cybernetics*, vol. 17, no. 4, pp. 211–220, 1975.

[15] A. Destexhe and T. J. Sejnowski, "The wilson–cowan model, 36 years later," *Biological cybernetics*, vol. 101, no. 1, pp. 1–2, 2009.

[16] R. M. Borisyuk and A. B. Kirillov, "Bifurcation analysis of a neural network model," *Biological Cybernetics*, vol. 66, no. 4, pp. 319–325, 1992.

[17] A. C. Marreiros, S. J. Kiebel, and K. J. Friston, "A dynamic causal model study of neuronal population dynamics," *Neuroimage*, vol. 51, no. 1, pp. 91–101, 2010.

[18] A. Borisyuk and J. Rinzel, "Understanding neuronal dynamics by geometrical dissection of minimal models," *Methods and Models in Neurophysics, Proceedings of Les Houches Summer School Elsevier*, pp. 19–72, 2005.

[19] P. Bressloff and S. Coombes, "Physics of the extended neuron," *International Journal of Modern Physics B*, vol. 11, no. 20, pp. 2343–2392, 1997.

[20] C. A. Schevon, S. A. Weiss, G. McKhann Jr, R. R. Goodman, R. Yuste, R. G. Emerson, and A. J. Trevelyan, "Evidence of an inhibitory restraint of seizure activity in humans," *Nature communications*, vol. 3, p. 1060, 2012.

[21] G. N. Borisyuk, R. M. Borisyuk, A. I. Khibnik, and D. Roose, "Dynamics and bifurcations of two coupled neural oscillators with different connection types," *Bulletin of mathematical biology*, vol. 57, no. 6, pp. 809–840, 1995.

[22] R. Borisyuk and Y. Kazanovich, "Oscillations and waves in the models of interactive neural populations," *Biosystems*, vol. 86, no. 1, pp. 53–62, 2006.

[23] M. Goodfellow, K. Schindler, and G. Baier, "Intermittent spike-wave dynamics in a heterogeneous, spatially extended neural mass model," *NeuroImage*, vol. 55, no. 3, pp. 920–932, 2011.

[24] S. Coombes and C. Laing, "Delays in activity-based neural networks," *Philosophical Transactions of the Royal Society A: Mathematical, Physical and Engineering Sciences*, vol. 367, no. 1891, pp. 1117–1129, 2009.

[25] A. Hutt and F. M. Atay, "Effects of distributed transmission speeds on propagating activity in neural populations," *Physical Review E*, vol. 73, no. 2, p. 021906, 2006.

[26] A. Roxin and E. Montbrió, "How effective delays shape oscillatory dynamics in neuronal networks," *Physica D: Nonlinear Phenomena*, vol. 240, no. 3, pp. 323–345, 2011.

[27] S. A. Campbell, "Time delays in neural systems," in *Handbook of brain connectivity*, pp. 65–90, Springer, 2007.

[28] Y. Kuznetsov, *Elements of Applied Bifurcation Theory*, vol. 112. Springer, 2004.

[29] A. Dhooge, W. Govaerts, Y. A. Kuznetsov, H. Meijer, and B. Sautois, "New features of the software matcont for bifurcation analysis of dynamical systems," *Mathematical and Computer Modelling of Dynamical Systems*, vol. 14, no. 2, pp. 147–175, 2008.

[30] J. Polking, *Ordinary Differential Equations Using MATLAB*. Pearson/Prentice Hall, 2004.

[31] K. Engelborghs, T. Luzyanina, and G. Samaey, "Dde-biftool v. 2.00: a matlab package for bifurcation analysis of delay differential equations," *TW Reports*, p. 61, 2001.